Optical Engineering

OpticalEngineering.SPIEDigitalLibrary.org

Stimulated Brillouin scattering in optical fibers with end reflections excited by broadband pump waves

Mark S. Bowers
Nicholas M. Luzod

SPIE.

Mark S. Bowers, Nicholas M. Luzod, "Stimulated Brillouin scattering in optical fibers with end reflections excited by broadband pump waves," *Opt. Eng.* **58**(10), 102702 (2019), doi: 10.1117/1.OE.58.10.102702.

Stimulated Brillouin scattering in optical fibers with end reflections excited by broadband pump waves

Mark S. Bowers* **and Nicholas M. Luzod**
Lockheed Martin Rotary and Mission Systems, Bothell, Washington, United States

Abstract. The transient theory of stimulated Brillouin scattering (SBS) in optical fibers is used to investigate the effects of weak feedback of incident broadband laser fields exhibiting different spectral shapes. The proper boundary conditions are given for the forward- and backward-propagating electric fields inside the fiber with a finite amount of reflectivity at the fiber ends. When the linewidth of the laser approaches the Brillouin frequency shift, a weak reflection of the laser field overlaps with the SBS gain and can be amplified in the fiber, resulting in an apparent reduction in SBS threshold. It is shown that the spectral shape of the incident field and its overlap with the SBS gain spectrum affects the SBS signal. Numerical examples are presented for incident laser fields that (1) simulate a pulsed, multilongitudinal-mode laser and (2) are a constant amplitude with a sinusoidal phase modulation. For the pulsed field with mode spacing much less than the Brillouin linewidth, calculations show that an end reflection of 0.01% (−40 dB) of the laser field with a linewidth equal to 0.75 of the Brillouin frequency shift can reduce the effective SBS threshold by a factor of 1.5. When the incident laser field is constant amplitude and phase modulated with a sinusoid, calculations predict sharp and distinct enhancement of the reflected power when the ratio of the Brillouin frequency shift to the modulation frequency is an integer for end reflections as low as 0.001% (−50 dB). Experiments performed with a sinusoidal phase modulated signal confirm the theoretical predictions. These results have implications on the design of high-power fiber laser systems that utilize spectral broadening to suppress SBS. © *The Authors. Published by SPIE under a Creative Commons Attribution 4.0 Unported License. Distribution or reproduction of this work in whole or in part requires full attribution of the original publication, including its DOI.* [DOI: 10.1117/1.OE.58.10.102702]

Keywords: stimulated Brillouin scattering; fiber lasers; fiber amplifiers; nonlinear fiber optics.

Paper 190359SS received Mar. 14, 2019; accepted for publication Jul. 10, 2019; published online Sep. 25, 2019.

1 Introduction

High power and narrow linewidth fiber amplifiers are desired for coherent and spectral beam combining approaches to scale the average output power beyond single-fiber limits.[1] The average power that can be achieved from a narrow linewidth fiber amplifier is typically limited by the nonlinear optical effect stimulated Brillouin scattering (SBS).[2] Various techniques have been used to suppress SBS in fiber lasers and amplifiers.[3] One technique for SBS suppression in amplifiers is to seed the fiber with laser radiation exhibiting a spectral width that exceeds the Brillouin linewidth. This can be achieved, for example, using a multimode laser for pumping. A more widely used technique to broaden the laser linewidth for SBS suppression is to externally modulate the laser radiation.[4] Using pure phase modulation techniques to broaden the laser linewidth is an attractive approach for high-average power operation because the linewidth can be directly controlled and the laser amplitude is constant in time. Pure phase modulation techniques have been used ranging from linear chirps,[5,6] white noise,[7,8] and periodic functions, such as pure sine waves,[9] pseudorandom binary sequences,[10] tailored periodic phase modulation generating a nearly top-hat shaped optical spectrum,[11] and periodic phase modulation patterns optimized for the highest SBS threshold at a given laser linewidth.[12] These techniques for broadening the laser linewidth can generate different spectral shapes, and the details of these shapes are important for SBS suppression.[13] Furthermore, the laser field is typically modulated at frequency levels near the Brillouin frequency shift, especially for high-power, Yb-doped fiber amplifiers that are used in beam-combining systems.[8,14,15]

As the bandwidth of the laser field is broadened and becomes comparable to the Brillouin frequency shift, it contains spectral components that overlap with the SBS gain. Therefore, a weak reflection of such a broadband laser field at the end of a fiber can act as a seed for the Stokes wave and becomes amplified in the SBS process, which can limit the achievable output power from a line-broadened fiber amplifier.[16,17] In essence, the fiber can transition from an SBS generator, where the Stokes wave is initiated from acoustic noise, to an SBS amplifier as the laser field is spectrally broadened and reflected back up the fiber. A small amount of feedback can be present in a fiber system from flat cleaves, endcaps, external backscatter, physical contact connectors, imperfect splices, or by splicing of a component exhibiting a small, yet finite, return loss. SBS in the presence of external feedback has been studied by others,[18,19] particularly for Brillouin fiber lasers;[20] however, the previous works considered single-frequency laser sources so that feedback of the laser field does not overlap with the SBS gain. For broadband laser fields with bandwidths comparable to the Brillouin frequency shift, a rigorous and accurate approach for predicting the effects of feedback is necessary to aid in setting limits on the amount of feedback that can be tolerated in a given fiber laser system.

In this paper, a rigorous approach is presented for simulating SBS in passive optical fibers pumped by a broadband laser field that includes the effects of feedback. The transient theory for SBS is used with the proper boundary conditions

*Address all correspondence to Mark S. Bowers, E-mail: mark.s.bowers@lmco.com

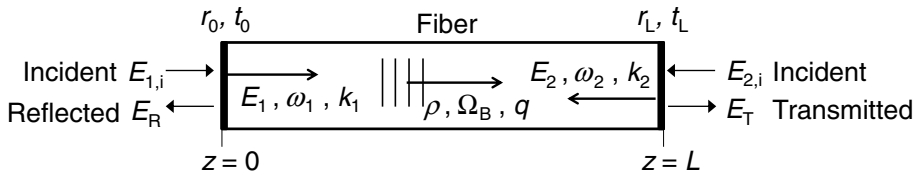

Fig. 1 Geometry for SBS in a passive fiber with reflectivity at both ends of the fiber. The incident pump wave is launched into the fiber at $z = 0$ and forward propagates from left to right. A backward-propagating wave can also be launched at $z = L$ for simulating an SBS amplifier.

for the forward- and backward-propagating fields in the time domain to include reflections of the fields from the fiber ends. Recently, theoretical formulations were developed that considered a reflection from only one end of the fiber.[16,21] In this work, the theory developed in Ref. 21 is extended to include reflections from both fiber ends with the possibility of injecting light into the fiber from either or both ends. This approach is general and can be applied to any modulated laser field for pulsed and CW systems and can also be used to simulate Brillouin lasers and amplifiers. To illustrate the utility of this theoretical approach, numerical results are presented to show the effects of weak feedback from the fiber end. The first example is a pulsed, periodic field incident on the fiber simulating emission from a laser oscillator with closely spaced longitudinal modes. For this pulsed field, it is shown that when the laser linewidth approaches the Brillouin frequency shift, a weak reflection of the laser field overlaps with the SBS gain and is then amplified in the SBS process. The fiber transitions from an SBS generator to an amplifier, which manifests itself as an effective decrease in SBS threshold and a reduction in the fluctuations of the SBS-generated reflected wave near threshold. In the example below, a 0.01% (−40 dB) reflection of a laser field with a linewidth equal to 0.75 of the Brillouin frequency shift is predicted to reduce the effective SBS threshold by as much as a factor of 1.5. The second example is for a monochromatic field that is phase modulated with a single-tone sinusoidal modulation function. In this case, the power spectrum of the incident field consists of a series of discrete frequency components at integer multiples of the modulation frequency. It is shown that for weak feedback from the fiber end, enhancement of the SBS process occurs when these discrete spectral laser lines overlap with the induced SBS gain spectrum. Section 4.1 describes experiments performed with sinusoidal phase modulation fields that confirm these theoretical predictions. These results can have implications on the design of high-power fiber laser systems that utilize spectral broadening to suppress SBS.

2 Theory

The transient theory of SBS is a rigorous approach for predicting SBS generation in a Brillouin-active material, such as optical fiber.[2,22] In this approach, SBS is described as a three-wave interaction of a laser (pump) wave, a Stokes wave, and an acoustic wave. In generators, the SBS process is initiated by spontaneous Brillouin scattering from thermally excited acoustic noise within the fiber.[22] In a Brillouin amplifier configuration, a Stokes wave is injected at the fiber end boundary that propagates in the opposite direction from the laser wave. The transient theory considers the finite temporal response of the medium and is able to predict the Stokes amplification and generation, Stokes linewidth, and fluctuations in Stokes wave as a function of the incident laser field and the physical properties of the Brillouin-active medium. The theory predicts the experimentally observed dynamic behavior of SBS in fibers with single-frequency laser pulses with durations on the same order as the phonon lifetime.[23,24] The transient theory has been used to theoretically investigate different modulation techniques for the suppression of SBS in optical fibers seeded with phase-modulated light, with the goal of achieving maximum SBS suppression with minimal linewidth broadening.[12,13]

The example geometry under consideration is a passive optical fiber with reflections at both ends, as shown in Fig. 1. An incident pump wave, denoted as $E_{1,i}$ in this figure, is launched into the fiber at $z = 0$ as a forward-propagating wave in the $+z$ direction. Similarly, an incident Stokes wave $E_{2,i}$ can be launched into the fiber at $z = L$ as a backward-propagating wave in the $-z$ direction. The interface at $z = 0$ is characterized by amplitude reflectivity and transmission coefficients r_0 and t_0, respectively. The boundary at $z = L$ reflects a portion of the forward-propagating field with amplitude reflectivity r_L in the counter-propagating $-z$ direction and transmits a portion with amplitude transmission t_L. Both interfaces at the fiber ends are assumed to be lossless such that $|r_0|^2 + |t_0|^2 = |r_L|^2 + |t_L|^2 = 1$.

In the present treatment, it is assumed that the reflections at the fiber ends are weak, i.e., the power reflectivities $R_L = |r_L|^2$ and $R_0 = |r_0|^2$ are much smaller than unity $(R_L, R_0 \ll 1)$. Therefore, all reflected field strengths are low and any anti-Stokes waves generated from the scattering of the backward-propagating laser field with the forward-propagating acoustic wave are ignored. For the same reason, any Brillouin interactions between a backward-propagating laser field and a forward-propagating Stokes field are neglected,[19] as is the generation of second-order Stokes through four-wave mixing and the second-order SBS process.[25] Thus only the Brillouin interaction between the forward-propagating laser field with a backward-propagating Stokes field is considered, which is valid as long as the end reflections are small.

The total electric field inside the Brillouin-active optical fiber is written as a sum of a forward-propagating field $\tilde{E}_1(z,t)$ and a backward-propagating field $\tilde{E}_2(z,t)$:

$$\tilde{E}_{\mathrm{TOT}}(z,t) = \tilde{E}_1(z,t) + \tilde{E}_2(z,t), \tag{1}$$

with the forward- and backward-propagating fields expressed in the following forms:

$$\tilde{E}_1(z,t) = \frac{1}{2} E_1(z,t) e^{i(k_1 z - \omega_1 t)} + \text{c.c.}, \tag{2}$$

and

$$\tilde{E}_2(z,t) = \frac{1}{2}E_2(z,t)e^{i(-k_2 z-\omega_2 t)} + \text{c.c.} \tag{3}$$

Here $E_1(z,t)$ and $E_2(z,t)$ are the complex slowly varying amplitudes, k_1 and k_2 are the wavenumbers, and ω_1 and ω_2 are the optical carrier frequencies for the forward-propagating and the backward-propagating fields, respectively. It is assumed that both the forward and backward fields are linearly polarized along the same direction and propagate in the fundamental transverse mode. The electric fields interact with each other in the fiber by means of the acoustic disturbance within the glass medium through the mechanism of electrostriction. This disturbance is described in terms of the change in the material density $\tilde{\rho}(z,t)$ from its mean value ρ_0, which is expressed in terms of a forward-propagating wave with its complex varying amplitude $\rho(z,t)$ according to

$$\tilde{\rho}(z,t) = \frac{1}{2}\rho(z,t)e^{i(qz-\Omega_B t)} + \text{c.c.}, \tag{4}$$

where the acoustic wavenumber q and angular frequency Ω_B are related to the forward- and backward-propagating field values through the conservation of momentum and energy by

$$q = k_1 + k_2 \tag{5}$$

and

$$\Omega_B = \omega_1 - \omega_2. \tag{6}$$

They are related to each other by the phonon dispersion relation $\Omega_B = qv$, where v is the velocity of sound in the glass medium.

Substituting Eqs. (2)–(4) into the Navier–Stokes equation and Maxwell's wave equations with the nonlinear polarization induced by electrostriction, and making the standard slowly varying amplitude approximation for the electric fields results in the following set of coupled equations:[13,26]

$$\frac{n}{c}\frac{\partial E_1(z,t)}{\partial t} + \frac{\partial E_1(z,t)}{\partial z} = \frac{i\omega\gamma_e}{4nc\rho_0}\rho(z,t)E_2(z,t), \tag{7}$$

$$\frac{n}{c}\frac{\partial E_2(z,t)}{\partial t} - \frac{\partial E_2(z,t)}{\partial z} = \frac{i\omega\gamma_e}{4nc\rho_0}\rho^*(z,t)E_1(z,t), \tag{8}$$

$$\frac{\partial^2\rho(z,t)}{\partial t^2} + (\Gamma - 2i\Omega_B)\frac{\partial\rho(z,t)}{\partial t} - i\Gamma\Omega_B\rho(z,t) = \frac{\gamma_e q^2}{ncS}E_1(z,t)E_2^*(z,t) - 2i\Omega_B f(z,t). \tag{9}$$

In Eqs. (7)–(9), the complex field amplitudes are normalized so that EE^* is the power of the fields, and the approximation $\omega = \omega_1 \simeq \omega_2$ is assumed. S is the effective mode area, n is the refractive index, c is the speed of light in vacuum, Γ is the phonon decay rate, and γ_e is the electrostrictive constant describing the change in the dielectric constant of the medium with respect to the change in the material density.[13] Linear absorption of the laser fields is neglected, and feedback due to Rayleigh backscattering along the fiber length is ignored, which is assumed to be small compared to the end reflections.[17]

The term $f(z,t)$ in Eq. (9) is the Langevin noise source for the initiation of the SBS process. It is assumed to be a Gaussian random variable with zero mean and δ correlated in space and time such that

$$\langle f(z,t)f^*(z',t')\rangle = A\delta(z-z')\delta(t-t'), \tag{10}$$

where the strength parameter A is derived from thermodynamic arguments for the thermal excitations of acoustic waves to be $A = 2k_B T\rho_0\Gamma/v^2 S$, where k_B is the Boltzmann's constant, and T is the temperature.[22]

For the evolution of the acoustic wave in Eq. (9), the derivatives in z are ignored as the acoustic wave moves slowly over the time scales of interest; however, the second-order derivative in time is retained. That is, the slowly varying envelope approximation is not invoked for the acoustic wave. The second derivative term should be retained when the laser pulse duration is shorter than the phonon lifetime or when the laser linewidth is on the order of the acoustic frequency,[27,28] which are the cases of interest in this work.

Equations (7)–(9) along with Eq. (10) with the appropriate boundary and initial conditions encompass the transient theory of SBS that has widely been used to study behavior of pulsed and CW laser sources in a Brillouin-active material.[2,12,13,16,18–24,26–30] In this work, the proper boundary conditions are presented to include reflections of broad bandwidth laser radiation.

The general form of the boundary conditions for the fields at $z = 0$ and $z = L$ can be obtained from an examination of Fig. 1, using Eqs. (2) and (3) for the electric fields inside the fiber, and by writing fields external to the fiber similar to Eq. (2) for the forward-propagating wave and Eq. (3) for the backward-propagating wave taking into account possible index of refraction changes at the boundaries. All forward-propagating waves internal or external to the fiber are written using ω_1 as the optical carrier frequency, and ω_2 is the optical carrier frequency for all backward-propagating waves. With these choices for the carrier frequencies, the boundary conditions at $z = 0$ are

$$E_1(z=0,t) = it_0 E_{1,i}(t) + r_0 E_2(z=0,t)e^{i\Omega_B t}, \tag{11}$$

$$E_R(t) = r_0 E_{1,i}(t)e^{-i\Omega_B t} + it_0 E_2(z=0,t), \tag{12}$$

where $E_{1,i}(t)$ is the complex electric field amplitude of the forward-propagating incident laser field at $z = 0$, and $E_R(t)$ is the complex electric field amplitude of the backward-propagating field reflected from the interface. The reflected field originates from a reflection of the incident laser field plus a backward-traveling wave transmitted at this interface. The coefficient $i = \sqrt{-1}$ in front of the transmission coefficient is the convention chosen here to ensure that the scattering matrix is unitary, and power is conserved at the interface.[31]

Similarly, the boundary conditions at $z = L$ are given by

$$E_2(z=L,t) = it_L e^{ik_2(1-\bar{n})L}E_{2,i}(t) + r_L e^{iqL}E_1(z=L,t)e^{-i\Omega_B t}, \tag{13}$$

$$E_T(t) = r_L e^{-i\bar{n}qL}E_{2,i}(t)e^{i\Omega_B t} + it_L e^{ik_1(1-\bar{n})L}E_1(z=L,t), \tag{14}$$

where $E_{2,i}(t)$ is the complex electric field amplitude of the backward-propagating laser beam launched into the fiber at $z = L$, $E_T(t)$ is the complex electric field amplitude of the forward-propagating field transmitted from this fiber end, and $\bar{n} = n_L/n$, where n_L the refractive index of the material to the right of the interface at $z = L$. The fixed phase terms on the right side of Eqs. (13) and (14) that include the fiber length L are overall phase shifts that depend on the choice of the origin $z = 0$. Such phase shifts may be important to include when the fields are resonating in a cavity, as in a Brillouin laser,[19,20] which is not considered here. They are retained in Eqs. (13) and (14) for completeness.

Equations (11)–(14) are expressions in the time domain for the boundary conditions linking the forward- and backward-propagating fields due to reflections from the fiber ends. For example, Eq. (13) expresses the backward-propagating wave inside the fiber at $z = L$ as the sum of a backward-propagating launched beam and the reflection of the forward-propagating wave at the fiber end. The $\exp(\pm i\Omega_B t)$ phase terms that are multiplied to the fields are due to the choice of the optical carrier frequencies ω_1 and ω_2 for the forward- and backward-propagating fields along with the conservation of energy expressed in Eq. (6). Equations (7)–(9) along with Eq. (10) and the boundary conditions Eqs. (11)–(14) constitute the transient theory of SBS with reflections of broadband laser fields at either end of a Brillouin-active medium for weak reflections from the fiber ends.

3 Numerical Examples

To illustrate the effects of feedback of broadband radiation with different spectral shapes on the SBS process, simulations were performed with different incident pump waves: a multimode pulsed laser and a monochromatic, continuous wave (CW) laser that is phase modulated with a single-tone sinusoidal function. Table 1 lists the parameters used to simulate SBS in a passive fiber pumped at a wavelength of 1064 nm. These parameters are the values for bulk silica glass and are typically used to simulate undoped silica fiber at a laser wavelength of 1064 nm.[2] Using these parameters, the commonly used Brillouin gain coefficient $g_B = \gamma_e^2\omega^2/(nc^3\rho_0\Gamma v)$ becomes 49.9 pm/W.

Table 1 Simulation parameters.

Parameter	Value
Wavelength	1064 nm
Density, ρ_0	2210 kg/m^3
Index of refraction, n	1.45
Acoustic velocity, v	5960 m/s
Phonon decay rate, $\Gamma/2\pi$	31.8 MHz
Electrostriction coefficient, γ_e	1.28
Brillouin frequency shift, $\Omega_B/2\pi$	16 GHz
Temperature, T	300 K
Mode area, S	3.14×10^{-10} m^2
Fiber length, L	8 m
Input power reflectivity, R_0	0

In both examples presented here, the power reflectivity at the input end is $R_0 = |r_0|^2 = 0$ to illustrate the effects of feedback on the SBS process from reflections at the output end of the fiber only when the incident laser field bandwidth approaches the Brillouin frequency shift. Configurations with weak feedback from both fiber ends have been studied previously with narrowband pump fields. These studies have shown that the threshold can be considerably lower than the threshold for SBS with no feedback,[19] and the Stokes intensity was found to exhibit various periodic, stable,[19] and even chaotic behaviors.[32] Even though the present theory can be used to predict these behaviors using either narrowband or broadband pump fields, weak feedback from both fiber ends is not considered in this paper.

The coupled complex amplitude equations, Eqs. (7) and (8), for the forward- and backward-propagating fields are numerically integrated in time and space in the fiber using the method of characteristics.[13] The fiber is discretized into a number of axial segments with length Δz, and the time step for the calculation is then set equal to the time required for light to propagate a distance of one axial segment, i.e., $\Delta t = n\Delta z/c$. Then Eqs. (7) and (8) for the fields involve only time derivates as the fields are integrated along a characteristic. The fields are advanced in time using standard ordinary differential equation numerical routines.

The acoustic wave satisfying Eq. (9) is advanced in time at each axial location along the fiber using an implicit first-order Euler method that is stable for all time steps.[33] This method is used because the equation can be somewhat stiff depending on the magnitudes of the Brillouin frequency shift and the phonon decay rate. For example, at a wavelength of 1 μm, the ratio Ω_B/Γ is nearly three orders of magnitude, and a stiff solver allows the use of larger time steps compared to standard numerical techniques, which reduces computational time while maintaining accuracy of the solutions. Results from the model were previously shown to compare well with experiments with no end reflections,[24] which establishes the validity of the calculations.

3.1 *Pulsed Laser Simulation*

A broadband incident laser field was simulated assuming the field emanates from a multilongitudinal-mode laser oscillator. The field was obtained by multiplication of a single frequency, temporally Gaussian pulse with a rapidly varying modulation signal, which was generated by adding multiple modes with independent complex Gaussian-distributed amplitudes and with an expectation spectrum corresponding to the desired laser spectral width. Specifically, the incident field is written as

$$E_{1,i}(t) = E_0 \exp\left[-\ln\sqrt{2}\left(\frac{t}{\tau_p/2}\right)^2\right]\sum_l A_l \exp(i\omega_l t), \quad (15)$$

where E_0 is a normalization constant determined from the pulse energy, τ_p is the full-width at half-maximum (FWHM) pulse width, A_l are the Gaussian-distributed complex amplitudes, and ω_l are the longitudinal-mode angular frequencies of the laser oscillator. For each laser pulse, the complex amplitudes were generated assuming a random phase and

amplitude so that each laser pulse exhibits different fine spectral details but within the desired Gaussian temporal envelope and specified spectral width. Inputs into the model are the laser pulse energy, FHWM pulse width τ_p, longitudinal-mode angular frequencies ω_l, and the FWHM laser linewidth defined as $\Delta\omega_L$.

For all simulation results in this section, the pulse width was fixed at 30 ns. The longitudinal-mode spacing of the incident laser field $(\Delta\omega = \omega_{l+1} - \omega_l)$ was taken as $\Delta\omega = 0.35\Gamma$; i.e., the mode spacing is smaller than the Brillouin gain bandwidth. Thus the SBS process will not be independent of the laser mode structure,[12,29] and this example illustrates a condition where an accurate determination of SBS can only be obtained from the transient theory. Such a small mode spacing can be generated from a long laser cavity, for example, a Q-switched fiber laser.

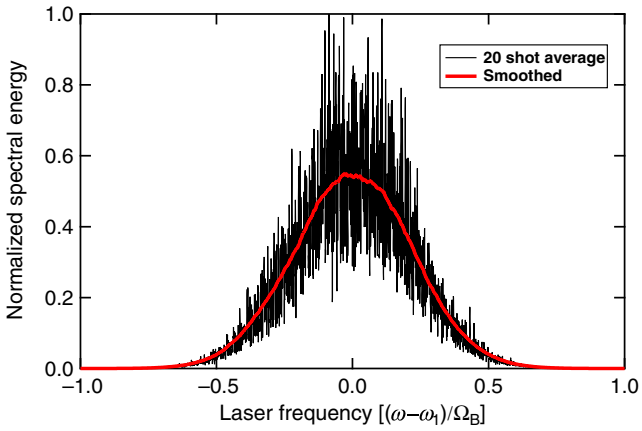

Fig. 2 Example incident laser spectrum averaged over 20 shots for FWHM frequency equal to half the Brillouin frequency shift $(\Delta\omega_L/\Omega_B = 0.5)$. Also shown is the spectrum smoothed using the resolution of a typical optical spectrum analyzer.

As SBS is initiated by the Langevin noise term and/or end reflections of a fluctuating laser field, the model results fluctuate, which is particularly noticeable near the threshold for an SBS generator. Therefore, the model results shown are an average over 20 laser pulses, unless otherwise noted. Each pulse has a different spatially distributed, fluctuating acoustic noise source, and each laser pulse is generated using randomly varying Gaussian-distributed complex amplitudes.

The bandwidth of the incident laser field was increased from a transform-limited pulse using the model for a multimode field in Eq. (15). An example of a computed incident spectrum averaged over 20 shots is shown in Fig. 2 for a FWHM laser linewidth equal to half the Brillouin frequency shift. Also shown is the averaged spectrum smoothed using the resolution from a typical optical spectrum analyzer. Many closely spaced longitudinal modes are included in the calculation with a smoothed average spectrum that is Gaussian in shape.

Figure 3(a) shows the predicted average reflected pulse energy divided by the incident laser pulse energy as a function of the incident pulse energy for a transform-limited, 30-ns pulse. The average pulse energy is the calculated pulse energy reflected back from the fiber averaged over 20 laser pulses. Curves are shown for different values of the power end reflectivity at $z = L$ ranging from $R_L = 0$ to $R_L = 10^{-3}$. For this small laser linewidth, there is no spectral overlap between the laser pulses reflected back through the fiber and the SBS gain. Thus the fiber acts as an SBS generator for all values of the end reflectivity. For small incident pulse energies (<1 μJ) and finite feedback (nonzero end reflections), the reflected energy is simply the incident light reflected at the fiber end that propagates back to the fiber input facet. As the incident energy increases, a back-propagating Stokes wave, shifted in frequency from the incident field by the Brillouin frequency shift, begins to grow and dominates the reflected signal. The curves for nonzero end

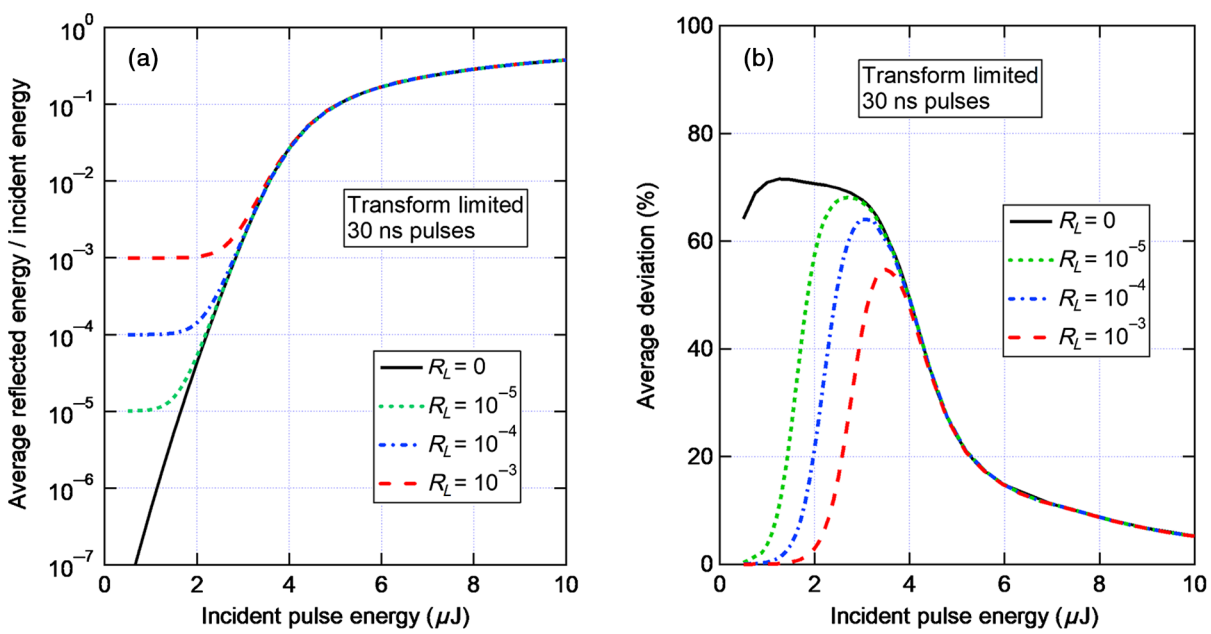

Fig. 3 Predicted (a) average reflected energy divided by the incident pulse energy and (b) average deviation from the mean of the reflected pulse energy as a function of incident energy for transform-limited, 30-ns pulses, and different power reflectivities at the fiber end. For a given incident pulse energy, the reflected pulse energy and deviation were computed by averaging over 20 laser pulses.

reflections are the sum of the $R_L = 0$ curve plus the end reflection value.

Fluctuations in the reflected pulse energy are shown in Fig. 3(b) for a transform-limited incident pulse and different values for the fiber end reflectivity. The measure of the fluctuations is presented in terms of the average deviation[33] of the reflected pulse energy from the mean value averaged over 20 pulses. The curve with no feedback is the predicted deviation in the backward-propagating Stokes field for an SBS generator. At low-incident pulse energy, the backward-propagating field is weak and exhibits large fluctuations, since the field is initiated from acoustic noise in the fiber. As the incident pulse energy is increased over 4 μJ, the SBS becomes saturated and the fluctuations in the backward-propagating Stokes tend to be suppressed due to pump depletion effects. The curves with finite end reflections exhibit low fluctuations for small incident pulse energies because the backward-propagating field is dominated by the reflection of the laser pulse at the fiber end, which is not fluctuating pulse to pulse for the input transform-limited pulses. As the pulse energy increases, the backward-propagating Stokes field begins to dominate over the reflected incident field, and eventually all curves approach the same values as the Stokes field increases.

Figure 4(a) shows the predicted average reflected energy as a function of incident pulse energy for a laser linewidth equal to 0.75 of the Brillouin frequency shift and for different values of the fiber end power reflectivity. For this large laser linewidth and with no feedback from the fiber end ($R_L = 0$), the fiber acts as an SBS generator with a predicted threshold ~70 times the threshold obtained with a transform-limited pulse, where threshold is defined when the average reflectivity is 0.01 (1%).

For small values of the fiber end reflections, however, the average reflected pulse energy in Fig. 4(a) is predicted to increase from the end reflection values near an incident pulse energy of 50 μJ and is always larger compared to the curve with no feedback. At the highest pulse energy of 600 μJ, the average reflectivity curves approach the same value because the SBS process becomes saturated. Again, defining the effective SBS threshold when the average reflectivity is 0.01, Fig. 4(a) shows that the effective threshold decreases as the end reflection value is increased. The higher average reflectivity at low-pulse energies and the reduction in the effective SBS threshold for finite end reflections is because the laser linewidth is broad enough to overlap with the SBS gain, and a fraction of the laser field reflected from the fiber end is amplified in the SBS process.

Figure 4(b) shows the predicted fluctuations in the backward-propagating pulse energy from the fiber for the broadband incident laser pulses corresponding to $\Delta\omega_L/\Omega_B = 0.75$. The fluctuations are largest for the SBS generator ($R_L = 0$) compared to those with small finite feedback for all incident pulse energies. This is because feedback of the incident broadband laser field seeds the SBS process rather than building up from noise. For incident pulse energies >500 μJ, the fluctuations become <10% for all feedback values because the SBS process becomes saturated in all cases.

The effects of increasing the laser linewidth for a fixed incident pulse energy of 250 μJ are shown in Fig. 5. In this example, 80 laser pulses were averaged. Without end reflections ($R_L = 0$), the reflected pulse energy steadily decreases as the laser linewidth increases, and the average reflectivity becomes very small ($< 10^{-2}$) for $\Delta\omega_L > 0.8\Omega_B$. With end reflections, the average reflected energy is the same as the $R_L = 0$ case for laser linewidths $\Delta\omega_L < 0.4\Omega_B$. However, as the linewidth approaches approximately half the Brillouin frequency shift, the reflected energy decreases less rapidly with end reflections compared to no end reflections. For a laser linewidth equal to the Brillouin frequency shift, there is still a measurable amount of SBS-generated reflected energy when end reflections are present, whereas the reflected energy for the SBS generator ($R_L = 0$) is over an order of magnitude smaller.

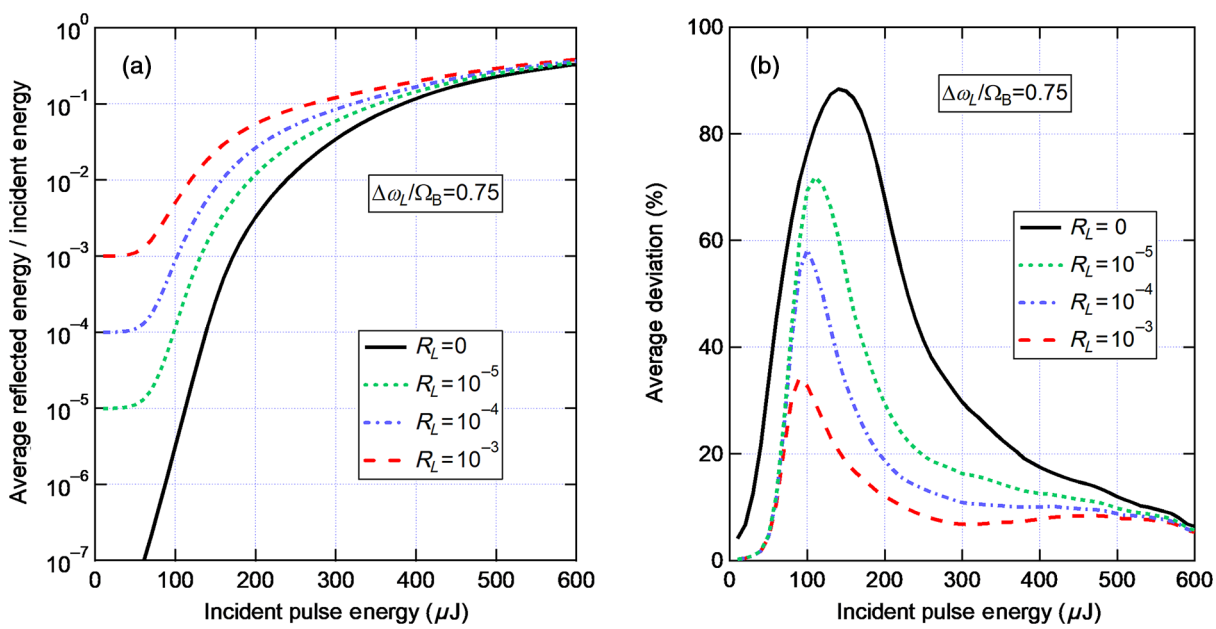

Fig. 4 Predicted (a) average reflectivity and (b) average deviation from the mean of the reflected energy as a function of incident pulse energy for a 30-ns laser pulse with FWHM linewidth equal to 0.75 of the Brillouin frequency shift.

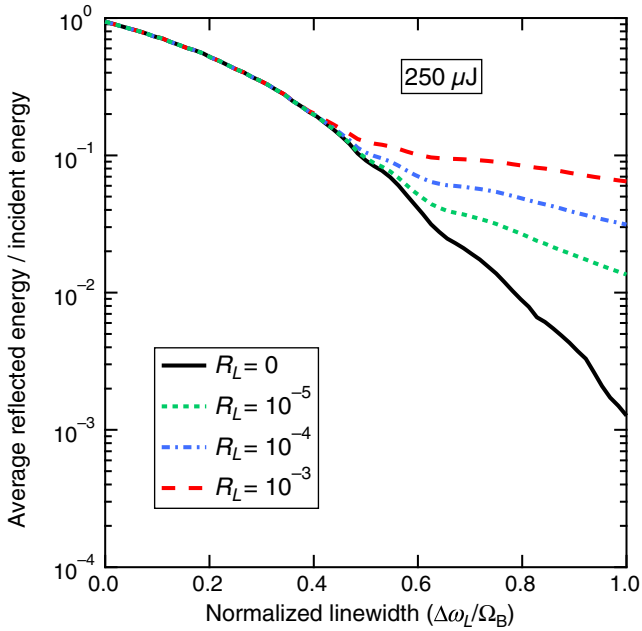

Fig. 5 The average reflected pulse energy divided by incident pulse energy as a function of normalized laser linewidth. Curves are for a fixed incident laser pulse energy of 250 μJ and different values of the end reflectivity averaged over 80 pulses. The laser pulse duration is 30 ns, and other parameters are listed in Table 1. A normalized bandwidth of 1 corresponds to a 16-GHz laser linewidth.

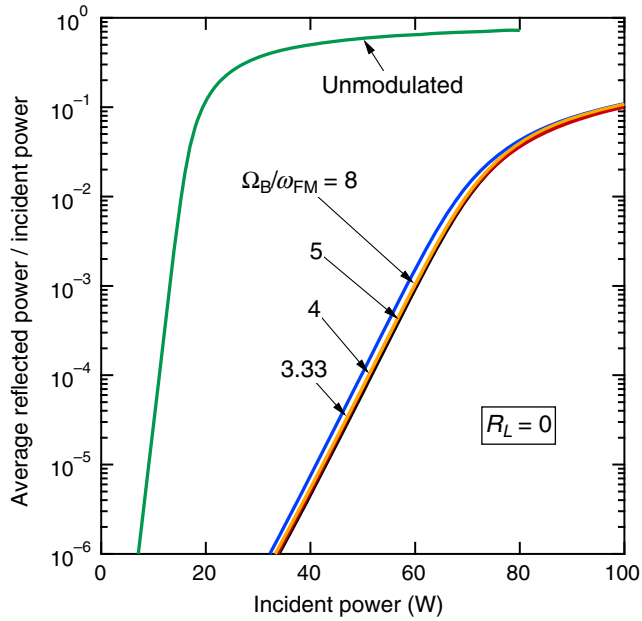

Fig. 6 Average reflected power divided by the incident power as a function of power incident on the fiber for various values of the sinusoidal modulation frequency normalized to the Brillouin frequency shift with the fiber end reflectivity $R_L = 0$. The numbers on the curves are the ratio of the Brillouin frequency shift to the modulation frequency.

From Fig. 5, it can be seen that the fiber acts as a saturated SBS generator for laser linewidths $\Delta\omega_L < 0.45\Omega_B$ with or without a small reflection from the fiber end for 250-μJ incident pulse energy. This is because in this regime, the reflected laser field spectrum does not overlap with the SBS gain, and the reflected field has no effect on the SBS process. However, for laser linewidths $\Delta\omega_L > 0.45\Omega_B$, the behavior of the SBS signal deviates from the $R_L = 0$ case when weak feedback is present. In this case, the laser spectrum begins to overlap with the SBS gain spectrum, the reflected field seeds the SBS process, and the fiber transitions from an SBS generator to an SBS amplifier. For large laser linewidths and weak feedback from the fiber end, the energy reflected at $z = 0$ is due to the amplification of the reflected laser field at $z = L$ resulting in higher energy and smaller fluctuations in the reflected output compared to the SBS generator ($R_L = 0$) behavior. These results are consistent with a previous study that showed a clamping of the SBS threshold pulse energy for laser linewidths $\Delta\omega_L > 0.45\Omega_B$.[21]

3.2 *Sinusoidal Phase Modulation*

The second numerical example is for a monochromatic field that is phase modulated with a single-tone sinusoidal modulation function. In this case, the power spectrum of the incident field consists of a series of discrete frequency components at integer multiples of the modulation frequency. The incident complex electric field is written as

$$E_{1,i}(t) = E_0 \exp[i\phi(t)], \tag{16}$$

where E_0 is a constant amplitude and the modulation function is given by

$$\phi(t) = \gamma \sin(\omega_{\mathrm{FM}} t). \tag{17}$$

Here γ is the modulation index and ω_{FM} is the modulation frequency. For the calculations presented in this section, the modulation index is fixed at $\gamma = \pi$, and the modulation frequency is varied from 0 up to about half the Brillouin frequency shift.

In all calculations in this section for a sinusoidal phase modulated field, the equations for the evolution of the fields in the fiber were integrated over 60 fiber transit times. The transmitted and reflected powers were time averaged over the last 30 fiber transit times.

Figure 6 shows the predicted average reflected power divided by the incident power as a function of the incident power for zero end reflections and different values of the modulation frequency. Different curves are shown for an unmodulated wave and for different ratios of the Brillouin frequency shift divided by the modulation frequency $\Omega_B/\omega_{\mathrm{FM}}$. For unmodulated radiation incident on the fiber ($\omega_{\mathrm{FM}} = 0$), the SBS threshold, defined as the laser power when the average reflectivity is 1%, is predicted to be 15.2 W, and the SBS process becomes saturated for incident powers >30 W reaching an average reflectivity of 72% at 80 W of incident power. The average reflectivity for the sinusoidal phase modulation fields all exhibit similar values as a function of the incident power. This is because at these large modulation frequencies, much larger than the Brillouin linewidth, the discrete spectral lines of the laser field act independently to generate SBS, and the highest power lines dominate the process independent of the modulation frequency.[13]

The behavior of the average reflectivity is much different when a small power reflection of $R_L = 10^{-5}$ is assumed at the fiber end, as shown in Fig. 7. For an unmodulated laser field incident on the fiber, the average reflected power as a

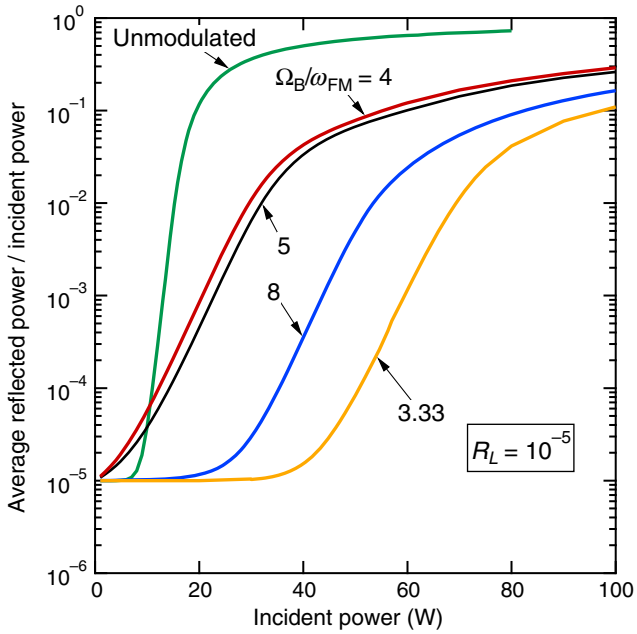

Fig. 7 Same as Fig. 6 with the fiber end reflectivity $R_L = 10^{-5}$.

function of incident power is identical to that with no end reflection shown in Fig. 6 apart from the finite value at low power (<10 W) due to the field reflected from the fiber end. Similarly, the average reflected power for a modulation frequency satisfying $\Omega_B/\omega_{\mathrm{FM}} = 3.33$ is nearly identical to the same curve with no end reflection in Fig. 6 for incident powers >50 W, approaching an average reflectivity value of 0.1 at 100 W of incident power. For these two cases, unmodulated and $\Omega_B/\omega_{\mathrm{FM}} = 3.33$, the reflection at the fiber end has no effect on the SBS process, and the fiber behaves as an SBS generator that is initiated by thermally excited acoustic noise. However, when the modulation frequency is such that the ratio $\Omega_B/\omega_{\mathrm{FM}} =$ integer, a small reflection of the laser field from the fiber end seeds the SBS process, the SBS threshold appears to decrease, and the fiber acts like an SBS amplifier,[30] as shown in the curves in Fig. 7 with modulation frequencies satisfying $\Omega_B/\omega_{\mathrm{FM}} = 4$, 5, and 8.

Figures 8(a) and 8(b) show the predicted transmitted and reflected powers as a function of the modulation frequency for a fixed incident power of 100 W. The power levels are normalized to the 100-W input power. In Fig. 8(a), there is no reflection from the fiber end ($R_L = 0$), and in Fig. 8(b), the fiber end reflection is $R_L = 10^{-5}$. For a single-frequency laser input $\omega_{\mathrm{FM}} = 0$, the fiber is well above the SBS threshold with an average reflectivity of 0.78. As expected, when the modulation frequency is increased, the transmitted power increases and the reflected power correspondingly decreases. The transmitted power initially rapidly increases to about 90 W, and, with no end reflections, there is minimal increase in the SBS suppression as the modulation frequency increases, as shown in Fig. 8(a).

With a small amount of power reflectivity at the fiber end of $R_L = 10^{-5}$, however, the reflected power shown in Fig. 8(b) is predicted to exhibit sharp and distinct enhancements, with a corresponding decrease in transmitted power, when the ratio of the Brillouin frequency shift to the modulation frequency is an integer. A closer examination indicates that the predicted width of the peak in the reflected power when $\Omega_B/\omega_{\mathrm{FM}} = 2$ is slightly less than half the Brillouin linewidth Γ. The widths of the other peaks at $\Omega_B/\omega_{\mathrm{FM}} = k$, where k is an integer, are $\sim 2/k$ times the width of the peak at $\Omega_B/\omega_{\mathrm{FM}} = 2$. Thus the widths of the peaks decrease as the integer ratio increases.

The reason for the resonant-like enhancement of the reflected power (and corresponding decrease in transmitted power) for $\Omega_B/\omega_{\mathrm{FM}} =$ integer can be most easily understood in the frequency domain. Figure 9 shows the predicted power

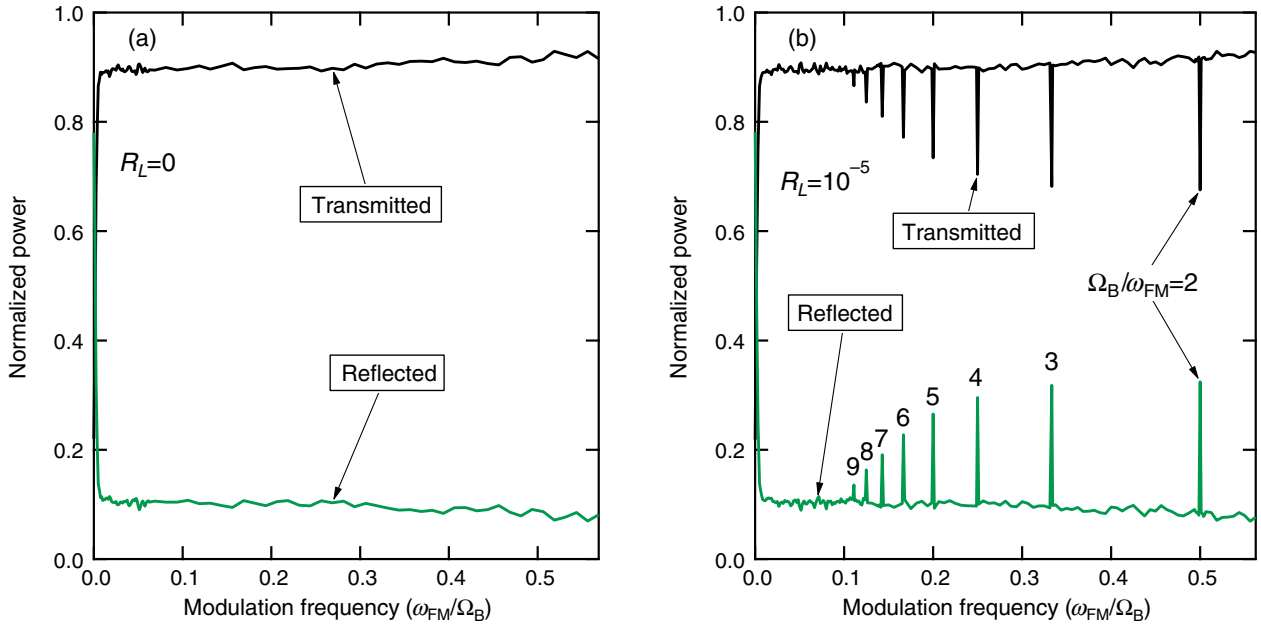

Fig. 8 Transmitted and reflected power, normalized to 100-W incident power, as a function of the modulation frequency for a sinusoidal phase modulated field with (a) no reflection from the fiber end ($R_L = 0$) and (b) with a small reflection of $R_L = 10^{-5}$.

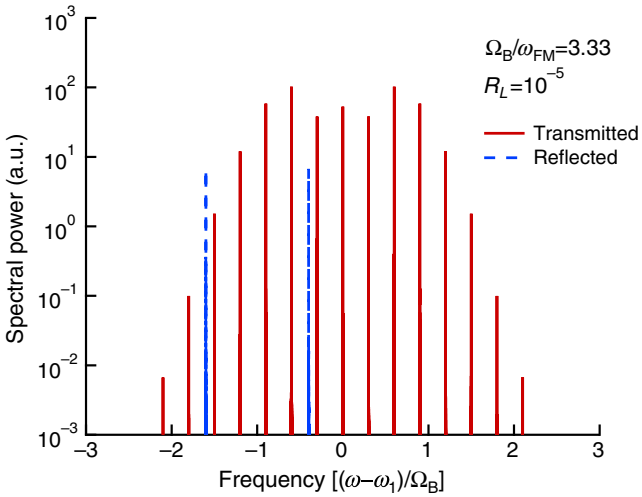

Fig. 9 Spectral power density of the transmitted and reflected fields as a function of normalized frequency for sinusoidal modulation frequency satisfying $\Omega_B/\omega_{\mathrm{FM}} = 3.33$ and fiber end reflection $R_L = 10^{-5}$. The frequency is centered about the input field carrier frequency and normalized to the Brillouin frequency shift, and the incident laser power is 100 W.

spectral density for the transmitted and reflected fields as a function of frequency normalized to the Brillouin frequency shift for 100-W incident on the fiber. The modulation frequency is such that $\Omega_B/\omega_{\mathrm{FM}} = 3.33$ with a fiber end reflection of $R_L = 10^{-5}$. In this case, the fiber is an SBS generator with the reflected field a Stokes wave initiated by thermally excited acoustic noise. The reflected Stokes wave is dominated by two spectral lines, which correspond to the two dominant incident laser field lines frequency downshifted by the Brillouin frequency shift.

Figure 10 shows the case when $\Omega_B/\omega_{\mathrm{FM}} = 4$ and $R_L = 0$ (no reflection from the fiber end). This is similar to the case in Fig. 9 except that the generated Stokes spectral lines now overlap with the incident laser field lines. Since there is no reflection from the fiber end, there is no seeding of the SBS process. However, Fig. 11 shows the large enhancement in the back reflected spectral power density when the SBS gain

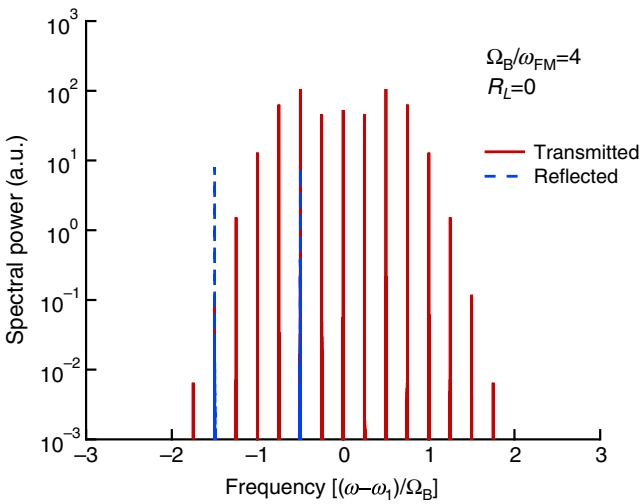

Fig. 10 Same as Fig. 9 for sinusoidal modulation frequency satisfying $\Omega_B/\omega_{\mathrm{FM}} = 4$ and fiber end reflection $R_L = 0$.

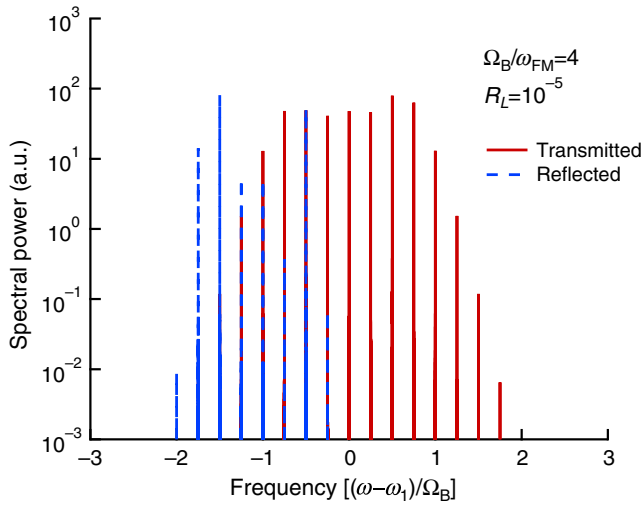

Fig. 11 Same as Fig. 10 for sinusoidal modulation frequency satisfying $\Omega_B/\omega_{\mathrm{FM}} = 4$ and fiber end reflection $R_L = 10^{-5}$.

overlaps with the incident laser field and a small amount of the laser field is reflected back up the fiber. In this case, the fiber acts as an SBS amplifier seeded by the reflected laser field, and the back-reflected spectrum consists of multiple lines with the same spacing between lines as the incident field.

As the modulation frequency is decreased, the enhancement of the reflected power decreases, as shown in Fig. 8(b), because the number of SBS gain spectral lines that overlap with the incident laser field lines decreases. This effectively reduces the amount of incident laser light that is fed back to seed the SBS process. Note, however, that even with a relatively small amount of feedback in Fig. 8(b), a large enhancement in the back-reflected power is predicted for modulation frequencies that are a small fraction of the Brillouin frequency shift.

4 Experiments

To test the theory, experiments were performed to measure the back-reflected power from a passive fiber pumped by a CW field that is phase modulated with a sinusoidal function. Reflected power as a function of launched power was measured for different modulation frequencies.

The experimental setup is shown in Fig. 12. CW output from a distributed-feedback diode laser operating at 1054 nm was phase modulated and then amplified in two fiber amplifier stages. The phase modulation was applied using a fiber-coupled lithium niobate phase modulator driven by a sine wave generator producing a single-tone sine wave, as in Eq. (17). A fiber-coupled tap coupler after the phase modulator transmitted ~99% of the light to two fiber amplifier stages, which boosted the power to a maximum of ~10 W. Both amplifier stages used Yb-doped, polarization-maintaining, single-mode, double-clad (8.7/125 μm core/cladding diameter) fiber. The output from the main amplifier was spliced to a fiber-coupled isolator and then to a 2×2, 99:1 tap coupler to measure both forward and backward power. The high-power port from the tap was spliced to a 12-m-long polarization-maintaining passive fiber (PM 980) to induce Brillouin scattering. For this experiment, the PM

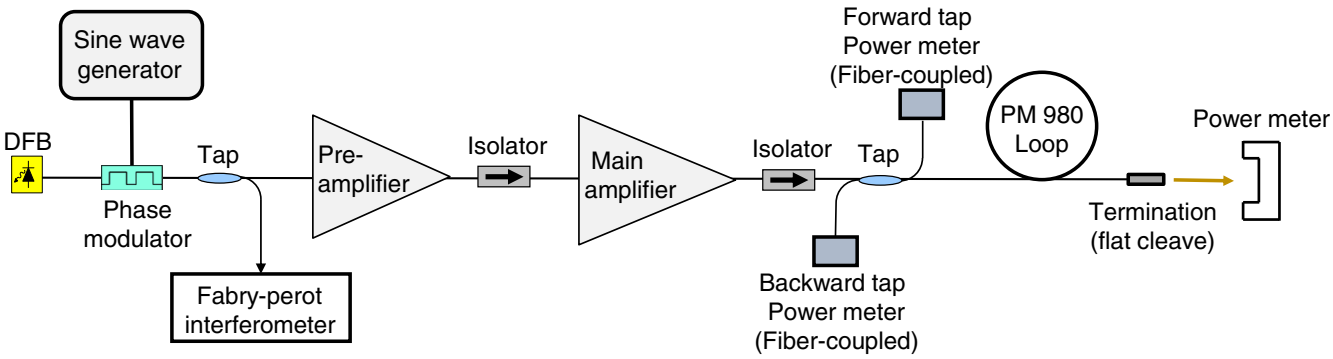

Fig. 12 Experimental setup to measure the SBS response from a length of PM 980 passive fiber pumped by a sinusoidal phase modulated signal. The continuous-wave output from a distributed feedback diode laser operating at 1054 nm is phase modulated with a sinusoidal function using an electro-optic phase modulator, which is then amplified in two stages of Yb-doped fiber amplifiers. A 2×2 tap coupler is spliced to the output of the main amplifier fiber and then to a 12-m length of PM 980 fiber. The forward tap measures the forward power launched into the PM 980 fiber, and the backward tap measures the back-reflected power.

980 was flat-cleaved at the output end to reflect ~3% of the light back into the PM 980 fiber core.

The tap coupler after the phase modulator sent a small amount of light to a Fabry–Pérot interferometer to measure the spectrum of the phase modulated signal. As the modulation frequency was varied, the RF amplitude to the phase modulator was adjusted to null out the carrier frequency in the spectrum. This ensures that the modulation index, γ in Eq. (17), was the same value for all modulation frequencies for comparing to the theory. The value of γ when the carrier frequency was nulled is the first zero of the Bessel function of the first kind of order 0, that is, $\gamma = 2.4048$.

The 2×2 tap coupling ratios were measured prior to the experiment, and splice loss was estimated by comparing the power with and without a short section of leader fiber spliced to the high-power port of the 2×2 tap. From these calibrations, the power launched into the PM 980 fiber was obtained from a measure of the forward tap power, and the backward-propagating power from the fiber core was obtained from the measured power at the backward tap.

4.1 *Experimental Results*

The modulation frequency was scanned at a lower power output from the amplifier of about 1 W, and backward power data were collected at each frequency step. A large enhancement in the backward power was observed when the modulation frequency was close to the expected value of the Brillouin frequency shift previously reported for silica glass, with the peak occurring at 16.02 GHz. Shifting the modulation frequency to integer fractions of 16.02 GHz also resulted in enhancements in the backward power, as predicted from the theory.

Figure 13 shows the measured reflected power divided by the launched power in percent as a function of the power launched into the PM 980 fiber for different modulation frequencies. For low incident power, the reflectivity is 3% for all modulation frequencies, which was the amount of light fed back into the fiber from the Fresnel reflection off of the flat-cleaved end. The data for the unmodulated wave $\omega_{\mathrm{FM}} = 0$ remained at 3% until the launched power reached a value of about 2.2 W, and for higher launched powers, the reflected power exponentially increased as expected from

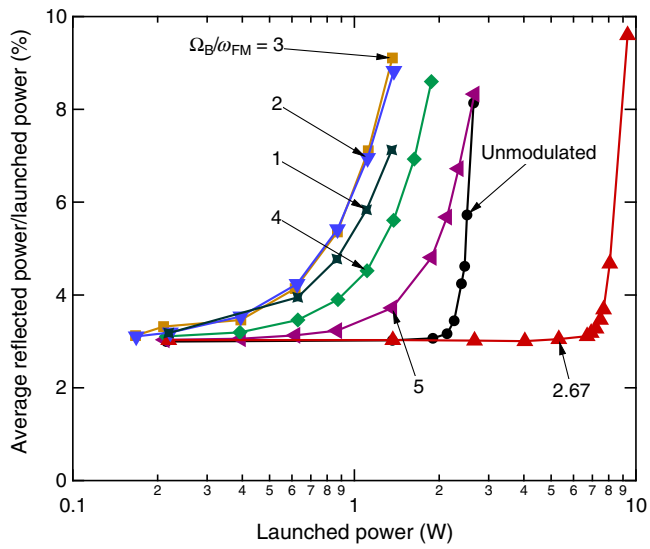

Fig. 13 Measured average reflected power divided by the launched power as a function of launched power for various values of the ratio $\Omega_B/\omega_{\mathrm{FM}}$. The Brillouin frequency shift is measured to be $\Omega_B/2\pi = 16.02$ GHz. The PM 980 fiber is terminated with a flat cleave, which extrapolates to a fiber end reflectivity $R_L = 0.03$ for small launched pump powers due to Fresnel reflections from the cleaved end. The numbered labels on the curves are the ratio of the Brillouin frequency shift to the modulation frequency.

an SBS generator. When the phase modulator was driven at 6 GHz, the ratio $\Omega_B/\omega_{\mathrm{FM}} = 2.67$ is a noninteger value; therefore, the spectrum of the light reflected from the cleaved end does not overlap with the SBS gain spectrum, and the effective SBS threshold power increased to about 7 W of launched power. The shape of the curve for $\Omega_B/\omega_{\mathrm{FM}} = 2.67$ is similar to the unmodulated curve shape. This is expected from theory since in both the $\Omega_B/\omega_{\mathrm{FM}} = 2.67$ and unmodulated situations, the SBS process in unseeded and thus the fiber acts as an SBS generator. The threshold enhancement factor for this modulated wave compared to the unmodulated wave is $(7/2.2) = 3.2$, which is comparable to the theoretical value of 3.71 determined from the sideband with the highest spectral power.[13]

When the modulation frequency was tuned such that the ratio $\Omega_B/\omega_{\mathrm{FM}} =$ integer, reflections from the cleaved end seeded the SBS process, and the SBS threshold effectively decreased. At these modulation frequencies, the fiber behaved as an SBS amplifier, as predicted by the theory. The measured back-reflected power at a given launched power depended on the amount of power reflected from the fiber end that overlaps with the SBS gain, which varied as the modulation frequency was tuned. Since the RF power to the phase modulator was adjusted as the modulation frequency was tuned to keep the modulation index constant, the spectral shape of the launched wave, and thus the fractional spectral power in the sidebands, was nearly the same at each modulation frequency. For this modulation index ($\gamma = 2.4048$), the reflected power for modulation frequencies satisfying $\Omega_B/\omega_{\mathrm{FM}} = 3$ and $\Omega_B/\omega_{\mathrm{FM}} = 2$ exhibited nearly the same values and generated the highest backward power for the lowest launched power, as shown in Fig. 13. Thus, at these two modulation frequencies, the fiber behaved as an SBS amplifier seeded with nearly the same power. Decreasing the modulation frequencies such that $\Omega_B/\omega_{\mathrm{FM}} = 4$ and $\Omega_B/\omega_{\mathrm{FM}} = 5$ resulted in a decrease in the backward power for a given launched power as expected; however, the SBS process was still seeded, and the apparent SBS threshold was decreased compared to the unmodulated results. The shape of the curves representing a modulation frequency tuned such that the ratio $\Omega_B/\omega_{\mathrm{FM}} =$ integer share a shallow slope rather than the steep exponential slope observed in the $\Omega_B/\omega_{\mathrm{FM}} = 2.67$ and the unmodulated conditions. The contrast in curve shapes shows the difference between SBS generators and SBS amplifiers. These results are clear experimental evidence that reflections from the fiber end seeded the SBS process when the modulation frequency is tuned such that the ratio of the Brillouin frequency shift to the modulation frequency is an integer.

4.2 *Simulation Results*

Calculations were performed to simulate the experimental conditions using the theory described in Sec. 2. Direct comparison to experiments was difficult since not all of the fiber parameters were known. Key fiber input parameters are the mode field diameter, Brillouin frequency shift Ω_B, SBS gain coefficient g_B, and the Brillouin linewidth Γ. The measured Brillouin frequency shift of 16.02 GHz was used as input to the model. It has been shown that the SBS gain coefficient in fiber differs from the bulk silica glass value due to the imperfect overlap between the electric field transverse modes and the acoustic modes in the fiber.[2,3] Measured values reported in the literature vary from 10 to 30 pm/W.[34] To estimate this gain coefficient, its value was varied until a good fit to the experimental data for the unmodulated wave was obtained. A value of 22.5 pm/W gave a good fit to the data using a mode-field diameter of 6.6 μm for the PM 980 fiber, which is within the range of SBS gain values reported in the literature. For the Brillouin linewidth, a value of $\Gamma/2\pi = 39$ MHz was used as this value was used previously to simulate SBS in PM 980 fiber.[34]

Calculations of the time-averaged backward power over several fiber transit times were performed with the reflection from the end facet of the 12-m-long fiber set at the experimentally determined value of $R_L = 0.03$. The modulation index was fixed at $\gamma = 2.4048$ and the modulation frequencies ω_{FM} were set to the experimental values. To adequately sample the phase modulation, the time steps were chosen to correspond to at least 40 points per modulation period. The total simulation time was at least 20 fiber transit times, and the backward power was averaged over the last half of the total integration time.

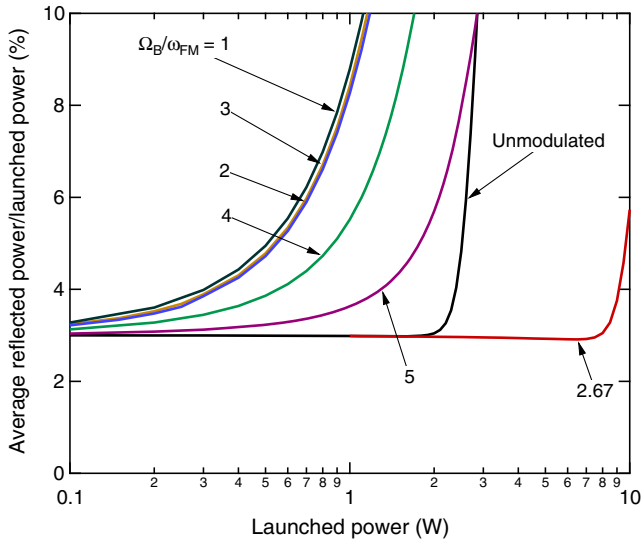

Fig. 14 Calculated average reflected power divided by the launched power as a function of launched power for various values of the ratio $\Omega_B/\omega_{\mathrm{FM}}$ simulating the experimental conditions shown in Fig. 13. The numbered labels on the curves are the ratio of the Brillouin frequency shift to the modulation frequency.

Figure 14 shows the results of the simulation, which are to be compared to Fig. 13. The calculations predict many of the trends observed in the experiments, including SBS enhancement for modulation frequencies tuned such that $\Omega_B/\omega_{\mathrm{FM}} =$ integer, and SBS suppression for the $\Omega_B/\omega_{\mathrm{FM}} = 2.67$ case. The average reflected power for modulation frequencies $\Omega_B/\omega_{\mathrm{FM}} = 3$ and $\Omega_B/\omega_{\mathrm{FM}} = 2$ is nearly the same, which is consistent with the experiments. The curves for lower modulation frequencies, $\Omega_B/\omega_{\mathrm{FM}} = 4$ and 5, follow the same order as the experiments. In addition, the model predicts the same curve shapes as the experimental results for all tested modulation frequencies. A close examination of the simulated and experimental data shows some disagreement. For instance, the simulation predicts that the highest backward power for the lowest launched power is achieved for a modulation frequency $\Omega_B/\omega_{\mathrm{FM}} = 1$, rather than the experimentally observed $\Omega_B/\omega_{\mathrm{FM}} = 3$. The difference between simulation and experiment might be attributed to the difficulty in experimentally tuning the modulation frequency exactly on resonance and errors in nulling the carrier frequency. In addition, the 2×2 tap coupler fiber was not included in the model, which may have resulted in a slightly different value for the SBS gain coefficient using the fitting procedure described above. A future parametric study of model inputs could be performed to determine the sensitivity of the model predictions to these experimental variables.

Though there are some differences between the experimental and simulation results, the simulations reproduce many of the measured trends with regard to SBS enhancement and the shape of the curves for both seeded and unseeded SBS conditions. These results again confirm seeding of the SBS process by a reflection at the fiber end when

the sinusoidal modulation frequency is such that $\Omega_B/\omega_{\mathrm{FM}} =$ integer.

5 Summary

In this paper, the transient theory of SBS was used to examine the effects of a small reflection of a broadband laser field at the output end of a Brillouin-active medium. The proper boundary conditions were derived in the time domain for the forward- and backward-propagating fields at the fiber ends. This formulation provides a rigorous approach for predicting the effects of weak reflections of incident broadband laser fields on the SBS process.

Example calculations were performed for a passive fiber pumped by (1) a broadband pulsed laser field consisting of closely spaced longitudinal modes with mode spacing smaller than the Brillouin gain bandwidth and (2) a constant amplitude, continuous-wave laser field that is broadened using sinusoidal phase modulation.

For the broadband pulsed laser field, the model predicts that when the laser linewidth is greater than about one half of the Brillouin frequency shift, the SBS process begins to transition from an SBS generator to an amplifier when the fiber end reflects a small amount of the laser field. As a result, a larger amount of reflected pulse energy is observed compared to the case with no feedback. For example, with a weak reflection of $R_L = 10^{-4}$ of the laser field with linewidth equal to 0.75 of the Brillouin frequency shift, the apparent SBS threshold is reduced by a factor of 1.5 compared to the case with no end reflection. Fluctuations of the SBS-generated reflected pulse energy is also reduced in the presence of laser field feedback.

For the constant amplitude, sinusoidal frequency-modulated laser field and small reflections of the incident field from the fiber end, the model predicts enhancement of the reflected power at discrete modulation frequencies when the SBS gain spectrum overlaps with the discrete spectral lines of the incident laser field spectrum. At these discrete frequencies, the laser field reflected back up the fiber seeds the SBS process, the SBS threshold appears to decrease, and the fiber acts like an SBS amplifier. Reflections as low as $R_L = 10^{-5}$ (-50 dB) can lead to large enhancements in the reflected power. Experiments were performed to confirm the theoretical predictions.

The reflectivities used in the calculations to illustrate the use of the theory varied from 10^{-3} to 10^{-5}, which are large compared to fiber amplifier systems with ends that are angle cleaved ($R_L < 10^{-6}$) or terminated with antireflection coatings. Smaller end reflections will result in less seeding of the SBS process, which will reduce the effects of feedback. The theory presented here can be used to quantify the impact of these smaller reflectivity values for a given line broadening function. Since all fiber systems will exhibit some amount of feedback, these results show that phase modulation parameters must be chosen properly to avoid overlap of the incident laser field spectrum with the SBS gain spectrum.

Acknowledgments

The authors gratefully acknowledge valuable discussions on the content of this paper with E. Honea, R. Afzal, D. Mordaunt, and M. Savage-Leuchs. Funding provided by Lockheed Martin Internal Research and Development.

References

1. S. J. Augst et al., "Beam combining of ytterbium fiber amplifiers," *J. Opt. Soc. Am. B* **24**, 1707–1715 (2007).
2. G. P. Agrawal, *Nonlinear Fiber Optics*, 5th ed., Elsevier, Waltham, Massachusetts (2013).
3. A. Kobyakov, M. Sauer, and D. Chowdhury, "Stimulated Brillouin scattering in optical fibers," *Adv. Opt. Photonics* **2**, 1–59 (2010).
4. F. W. Willems, J. C. van der Plaats, and W. Muys, "Simultaneous suppression of stimulated Brillouin scattering and interferometric noise in externally modulated lightwave AM-SCM systems," *IEEE Photonics. Technol. Lett.* **6**, 1476–1478 (1994).
5. J. O. White et al., "Suppression of stimulated Brillouin scattering in optical fibers using a linearly chirped diode laser," *Opt. Express* **20**, 15872–15881 (2012).
6. E. Petersen et al., "Stimulated Brillouin scattering suppression with a chirped laser seed: comparison of dynamic model to experimental data," *IEEE J. Quantum Electron.* **49**, 1040–1044 (2013).
7. A. Mussot, M. L. Parquier, and P. Szriftgiser, "Thermal noise for SBS suppression in fiber optical parametric amplifiers," *Opt. Commun.* **283**, 2607–2610 (2010).
8. G. D. Goodno et al., "Active phase and polarization locking of a 1.4 kW fiber amplifier," *Opt. Lett.* **35**, 1542–1544 (2010).
9. T. Torounidis, P. A. Andrekson, and B. Olsson, "Fiber-optical parametric amplifier with 70-dB gain," *IEEE Photonics Technol. Lett.* **18**, 1194–1196 (2006).
10. C. Robin et al., "Pseudo-random binary sequency phase modulation in high power Yb-doped fiber amplifiers," *Proc. SPIE* **8601**, 86010Z (2013).
11. A. V. Harish and J. Nilsson, "Optimization of phase modulation with arbitrary waveform generators for optical spectral control and suppression of stimulated Brillouin scattering," *Opt. Express* **23**, 6988–6999 (2015).
12. A. V. Harish and J. Nilsson, "Optimization of phase modulation formats for suppression of stimulated Brillouin scattering in optical fibers," *IEEE J. Sel. Top. Quantum Electron.* **24**, 1–10 (2018).
13. C. Zeringue et al., "A theoretical study of transient stimulated Brillouin scattering in optical fibers seeded with phase modulated light," *Opt. Express* **20**, 21196–21213 (2012).
14. E. Honea et al., "Spectrally beam combined fiber lasers for high power, efficiency, and brightness," *Proc. SPIE* **8601**, 860115 (2013).
15. S. M. Redmond et al., "Diffractive coherent combining of a 2.5 kW fiber laser array into a 1.9 kW Gaussian beam," *Opt. Lett.* **37**, 2832–2834 (2012).
16. B. M. Anderson, A. Flores, and I. Dajani, "Filtered pseudo random modulated fiber amplifier with enhanced coherence and nonlinear suppression," *Opt. Express* **25**, 17671–17682 (2017).
17. V. Balaswamy et al., "Experimental analysis of stimulated Brillouin enhancement in high power, line-broadened, narrow-linewidth fiber amplifiers due to spectral overlap between the Brillouin gain spectrum and the signal back-scatter from the fiber termination," *Proc. SPIE* **10902**, 10902G (2019).
18. M. Dämmig et al., "Stimulated Brillouin scattering in fibers with and without external feedback," *Phys. Rev. A* **48**, 3301–3309 (1993).
19. A. L. Gaeta and R. W. Boyd, "Stimulated Brillouin scattering in the presence of external feedback," *Int. J. Nonlinear Opt. Phys.* **1**, 581–594 (1992).
20. V. Lecoeuche et al., "Dynamics of stimulated Brillouin scattering with feedback," *Quantum Semiclassical Opt.* **8**, 1109–1145 (1996).
21. M. S. Bowers and R. S. Afzal, "Stimulated Brillouin scattering in optical fibers excited by broad-band pump waves in the presence of feedback," *Proc. SPIE* **8733**, 873301 (2013).
22. R. W. Boyd, K. Rzazwski, and P. Narum, "Noise initiation of stimulated Brillouin scattering," *Phys. Rev. A* **42**, 5514–5521 (1990).
23. H. Li and K. Ogusu, "Dynamic behavior of stimulated Brillouin scattering in a single-mode optical fiber," *Jpn. J. Appl. Phys.* **38**, 6309–6315 (1999).
24. M. Savage-Leuchs, M. S. Bowers, and A. J. W. Brown, "Stimulated Brillouin scattering in multimode fibers," *Proc. SPIE* **4972**, 145–150 (2003).
25. T. H. Russell and W. B. Roh, "Threshold of second-order stimulated Brillouin scattering in optical fiber," *J. Opt. Soc. Am. B* **19**, 2341–2345 (2002).
26. A. A. Fotiadi et al., "Statistical properties of stimulated Brillouin scattering in single-mode optical fibers above threshold," *Opt. Lett.* **27**, 83–85 (2002).
27. G. Grosso and A. Höök, "Generation of short pulses by stimulated Brillouin scattering in optical fibers," *J. Opt. Soc. Am. B* **10**, 946–951 (1993).
28. L. Ren and Y. Tomita, "Transient and nonlinear analysis of slow-light pulse propagation in an optical fiber via stimulated Brillouin scattering," *J. Opt. Soc. Am. B* **26**, 1281–1288 (2009).
29. P. Narum, M. D. Skeldon, and R. W. Boyd, "Effect of laser mode structure on stimulated Brillouin scattering," *IEEE J. Quantum Electron.* **22**, 2161–2167 (1986).
30. M. S. Bowers, "Stimulated Brillouin scattering in optical fibers with end reflections excited by broad-band, phase-modulated pump waves," *Proc. SPIE* **9466**, 94660J (2015).

31. A. E. Siegman, *Lasers*, University Science Books, Sausalito, California (1986).
32. S. H. Lee, D.-S. Lee, and C.-M. Kim, "Chaotic stimulated Brillouin scattering near the threshold in a fiber with feedback," *Opt. Express* **15**, 524–529 (2007).
33. W. H. Press et al., *Numerical Recipes in FORTRAN: The Art of Scientific Computing*, 2nd ed., Cambridge University Press, New York (1992).
34. G. L. Keaton et al., "Stimulated Brillouin scattering of pulses in optical fibers," *Opt. Express* **22**, 13351–13365 (2014).

Mark S. Bowers received his BS degree in physics from Pacific Lutheran University in 1981 and his MS and PhD degrees in physics from the University of California, Riverside, in 1983 and 1986, respectively. He is a technical fellow at Lockheed Martin. His current research interests include nonlinear fiber optics, fiber lasers and amplifiers, and nonlinear frequency conversion. He is a senior member of SPIE and the Optical Society of America.

Nicholas M. Luzod received his BS degree in biomedical and electrical engineering from Boston University in 2012 and his MS degree in optical sciences from the University of Arizona in 2016. He is an optical engineer at Lockheed Martin. He currently works on the development of fiber lasers and free space optical systems.